IEEE Access
Multidisciplinary ⋮ Rapid Review ⋮ Open Access Journal

Received 29 May 2025, accepted 18 June 2025, date of publication 24 June 2025, date of current version 14 July 2025.

Digital Object Identifier 10.1109/ACCESS.2025.3582429

RESEARCH ARTICLE

Vibration Control and Performance Analysis of a 3DOF High-Payload Flexible Link Manipulator

THIERRY HUBERT[1,2], AMIN KHORASANI[1,2], MUHAMMAD USMAN[1,2], HAFSA NOUHI[1,2], RAPHAËL FURNÉMONT[1,3], JOHN LATAIRE[4], (Member, IEEE), BRAM VANDERBORGHT[1,2], GREET VAN DE PERRE[1,2], AND TOM VERSTRATEN[1,3], (Member, IEEE)

[1]BruBotics, Vrije Universiteit Brussel, 1050 Brussels, Belgium
[2]Imec, 3001 Leuven, Belgium
[3]Flanders Make, 3920 Lommel, Belgium
[4]Research Group Fundamental Electricity and Instrumentation, Vrije Universiteit Brussel, 1050 Brussels, Belgium

Corresponding author: Thierry Hubert (thierry.rene.hubert@vub.be)

This work was supported by the Research Foundation Flanders (FWO) Strategisch Basis Onderzoek (SBO) Project Energy-efficient Lightweight Yet Strong Arm (ELYSA) Project under Grant S001821N, Grant 12Z7920N.

ABSTRACT Flexible link manipulators (FLMs) are often praised for their potential advantages in industrial settings, such as being more lightweight, energy-efficient, and allowing higher operation speeds with smaller actuators. Many studies make unrealistic assumptions, like simplistic links, small deflections, low payloads, limited degrees of freedom, and well-defined mode shapes, which limit their real-world applicability. This paper investigates the performance of a flexible link manipulator with three degrees of freedom, designed for high payload capabilities and characterized by complex link shapes and complex vibration modes. An advanced control methodology was developed following the identification of the parameter-varying flexible link manipulator setup to manage the manipulator's vibrations effectively. Comparative experiments were conducted between the flexible link manipulator and a conventional rigid link manipulator, assessing performance metrics such as repeatability, overshoot, settling time, torque and energy consumption. The results show that the flexible link manipulator, equipped with the advanced control system, achieves a repeatability of 0.14 mm, comparable to that of commercially available rigid robots. Moreover, energy consumption is reduced even with the implementation of active vibration suppression. The study highlights the potential of flexible link manipulators for real-world applications.

INDEX TERMS Vibration control, flexible links, repeatability, energy consumption.

I. INTRODUCTION

Flexible link manipulators (FLM) are often praised for their many potential advantages in industrial settings. FLMs have the potential to be more lightweight and energy efficient, and to allow higher operation speeds and the use of smaller actuators [1], [2], [3], [4], [5], [6]. However, flexible links are almost exclusively discussed in a research setting, where either modelling or control are prioritised. In addition to that, many of the studies performed on flexible links make unrealistic assumptions, e.g. simplistic links, small deflections, low payloads, low degrees of freedom, and well-defined mode shapes, limiting their applicability in real-world scenarios [1], [2], [3], [4], [5], [6]. It is essential to develop more realistic FLM and experimental setups that account for the complexities of real-world applications to understand and mitigate complex vibration responses. This includes considering high and varying payloads, complex link shapes, higher degrees of freedom, and complex vibration responses.

Examples are present in literature where researchers tend to focus on individual setups to address the specific complexities mentioned above, without combining all assumptions into a single robotic system. This fragmented approach limits the applicability of research findings to real-world scenarios, where flexible link manipulators must simultaneously handle multiple complex factors and perform under diverse conditions [4]. Table 1 provides a structured overview of

The associate editor coordinating the review of this manuscript and approving it for publication was Zhengmao Li.

TABLE 1. Overview of literature on flexible link manipulators. This table summarizes key literature relevant to our study, highlighting their addressed topics and identifying existing shortcomings. The identified gaps in the literature (such as complex link shapes, low degree of freedom, low payloads, and vibrations patterns) are outlined, along with an indication of whether these challenges have been experimentally validated or remain unaddressed.

non-uniform link(s)	DOF>2	Payload > 0.5kg	Direction of the vibrations	Successful experimental validation	Reference
			⊥	X	[7]–[12]
	X		// ⊥		[13]
			⊥		[14]
	X	X	⊥	X	[15]
			⊥	X	[16]
X*	X		//	X	[17], [18]
			// ⊥	X	[19], [20]
X			⊥	X	[21]
		X	⊥	X	[22]
X	X	X	//	X	This paper

*rigid links
⊥ vibrations perpendicular to the axis of rotation
// vibrations parallel to the axis of rotation

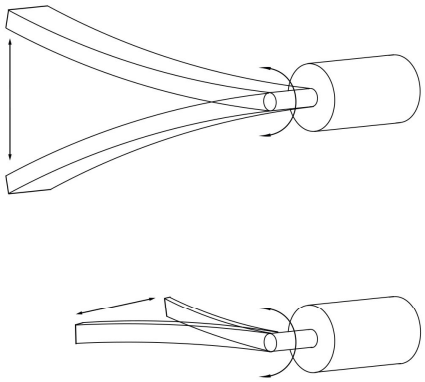

FIGURE 1. Vibration perpendicular to the axis of rotation (top). Vibration parallel to the axis of rotation (bottom).

TABLE 2. DH-parameters of the experimental setups. Values based on the Kuka iiwa robot.

	θ [rad]	a [mm]	d [mm]	α [rad]
Joint 1	θ_{j1}	0	200	$\pi/2$
Joint 2	θ_{j2}	420	0	0
Joint 3	θ_{j3}	400	0	0

TABLE 3. Properties of the experimental setups, showing a 3DOF high payload FLM with optimized lightweight links.

	flexible links	rigid links
Degrees of freedom	3	3
Payload [kg]	10	10
Reach* [mm]	820	820
Link 1 length* [mm]	200	200
Link 2 length* [mm]	420	420
Link 3 length* [mm]	400	400
Mass link 2 [kg]	0.59	3.84
Mass link 3 [kg]	0.47	2.5
Total mass [kg]	18.4	23.32

*Consistent with DH-parameters

the literature on flexible manipulators, highlighting the key limitations that our work aims to address in its entirety and comprehensively.

A. LINKS

In research, flexible links are modelled as simplified beams, often with uniform cross-sections and homogeneous mass distribution. This approach is primarily done because simple beams are mathematically tractable and provide a clear understanding of fundamental principles such as deformation, vibration, and dynamic behaviour [3], [5]. The use of simple beam models allows researchers to leverage well-established mathematical tools and theories, such as Euler-Bernoulli, Timoshenko beam theories and assumed modes method, to derive analytical solutions for bending, torsion, and dynamic responses. These models make it easier to predict how the link will behave under various loads and constraints. In contrast, real-world industrial robots have links with complex geometries tailored to specific tasks and operational environments. These practical designs often feature curved surfaces, varying cross-sections, and integrated components such as sensors, actuators, and cabling [3], [5]. Table 1 highlights studies that predominantly utilize simple link geometries, often rectangular or cylindrical in shape. More complex structural designs are rarely explored, and when they are, they are typically considered as rigid rather than flexible. This paper defines a complex link shape as one that exhibits a non-uniform cross section and/or a non-homogeneous distribution of mass.

B. PAYLOAD

In flexible link research, the inclusion or exclusion of payloads, and the size of those payloads, significantly impact the findings and their applicability to real-world scenarios [1], [7]. By eliminating or minimising the payload, researchers can isolate and study the fundamental effects of flexibility, such as natural frequencies, and modes of vibration. However, these can all change depending on the payload [23]. In the literature of Table 1, no payloads exceed 1 kg, with average tested payloads around 200 g, limiting the relevance of these studies for high-load applications and real-world applications. Additionally, larger payloads can introduce non-linear effects, such as large deformations and

TABLE 4. Estimated fundamental frequencies with their respective damping ratios for G_{FLM} when $\theta_{j2} = -90°$, $\theta_{j3} = 0°$ and $m_{pl} = 10$ kg.

Fundamental frequencies			Damping ratio		
f1 [Hz]	f2 [Hz]	f3 [Hz]	$\zeta 1[ul]$	$\zeta 2[ul]$	$\zeta 3[ul]$
1.45	5.74	9.89	0.0076	0.0113	0.0074

non-linear scaling behaviour, complicating the analysis and modelling [3], [24].

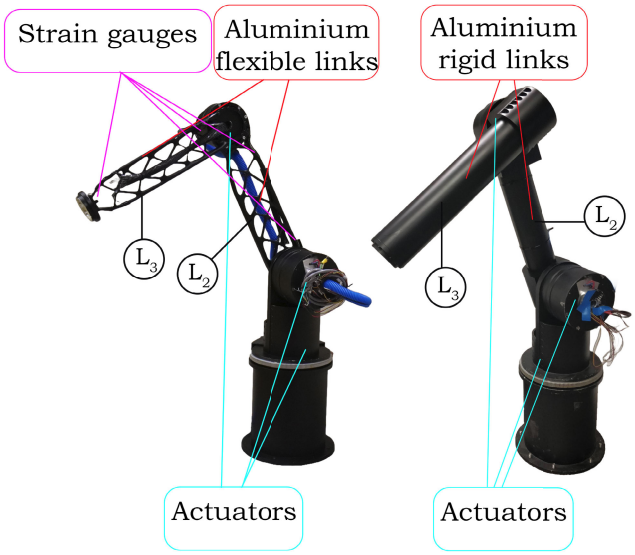

FIGURE 2. The experimental setup used for comparing a flexible link manipulator (left) and a rigid link manipulator with hollow cylindrical links (right). There is no payload on either end effector in this figure.

C. DEGREE OF FREEDOM

Research often concentrates on single flexible links rather than multi-link systems, primarily to simplify the analysis and gain a fundamental understanding of how flexibility influences robotic behaviour [1], [5]. However, this focus on single links may not fully represent the complexities of real robotic systems. Many real-world robotic systems require multiple degrees of freedom (DOF) to function effectively, and the dynamics of these systems can be significantly more complex than those of single-link systems. Multi-link systems often exhibit emergent behaviours arising from the interactions between individual links, which cannot be adequately represented by studying single links in isolation. Additionally, interactions between links, such as vibration coupling and transmission of reaction forces, are crucial in multi-link systems but may be overlooked in single-link studies. To address this gap, researchers are gradually incorporating multi-link studies into their research, starting with simpler two-link systems and scaling up as their understanding grows [1], [6], [25]. Advanced simulation and modelling techniques, such as multi-body dynamics simulations, enable researchers to explore system-level effects and interactions in multi-link systems more comprehensively. Experimental validation using realistic testbeds that replicate real-world

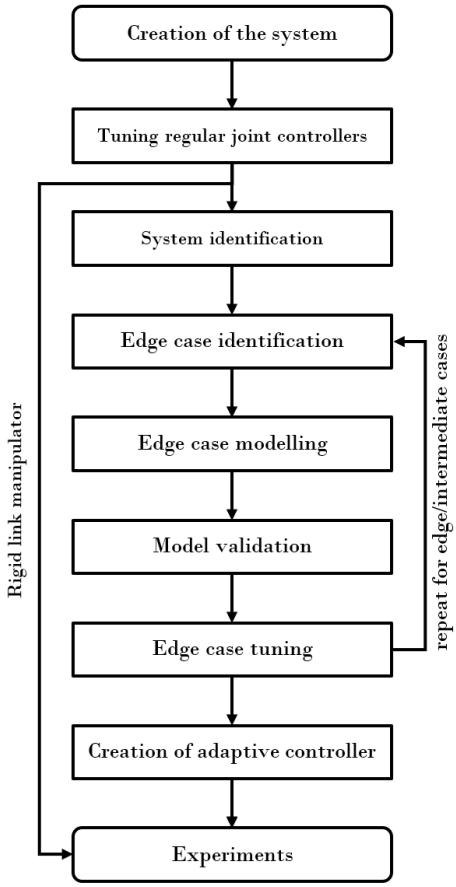

FIGURE 3. Flowchart for developing an adaptive controller for a flexible link manipulator to reduce vibrations.

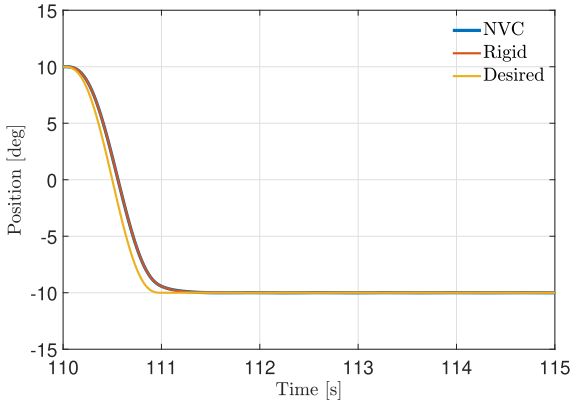

FIGURE 4. Example comparability of position of joint 1 following a step trajectory with payload of 10 kg and a max end effector speed of 1.5 m/s. Robustness of the controller showed a difference of maximum 0.004° between the RLM and FLM, following a smoothened step trajectory.

conditions, including multi-link systems with flexible components, is also essential for validating theoretical models and simulation results [6], [25]. By integrating multi-link studies, advanced simulation techniques, and experimental validation approaches, researchers can develop a more comprehensive understanding of how flexibility impacts the performance of multi-link robotic systems, advancing the design, control, and

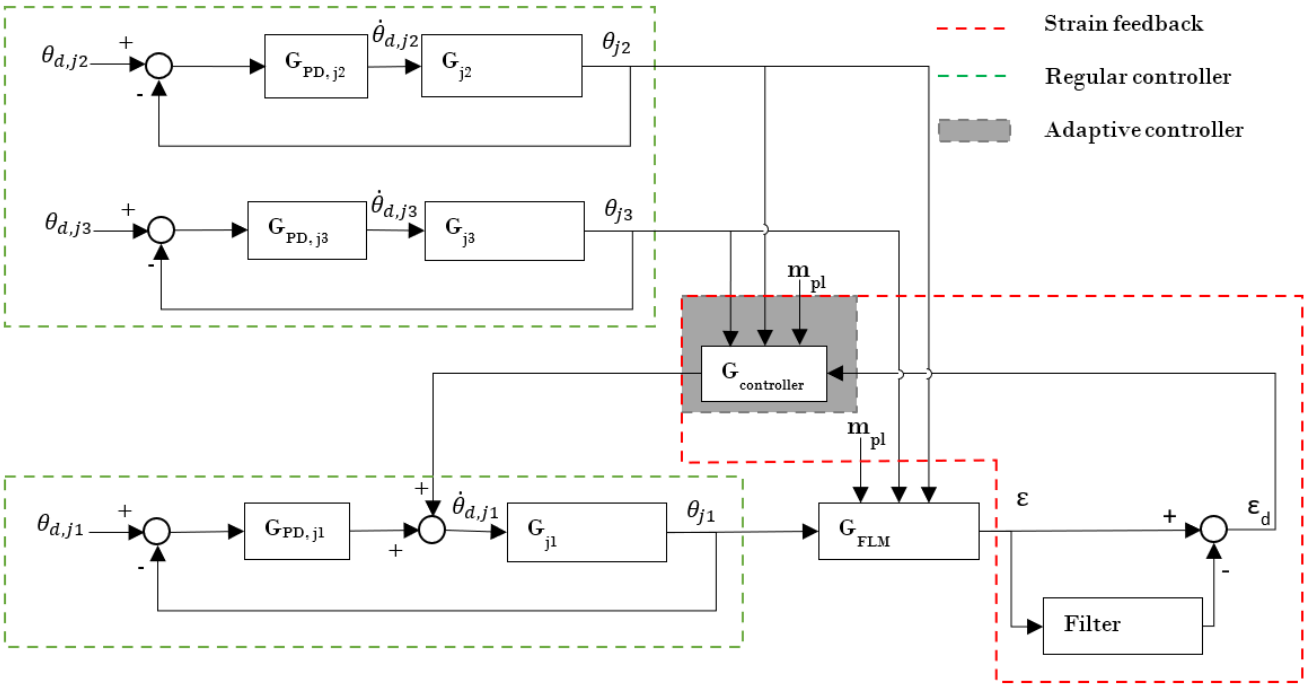

FIGURE 5. Control schematic of the flexible link manipulator for vibration control, including a strain feedback and adaptive controller on joint 1. The rigid manipulator only uses the regular velocity controller.

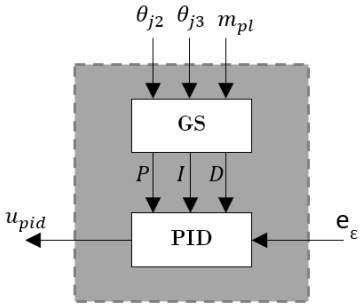

FIGURE 6. Breakdown of the adaptive controller, featuring a gain scheduler that is dependent on the joint positions and the payload. This gain scheduler supplies the PID values for the PID strain-feedback controller.

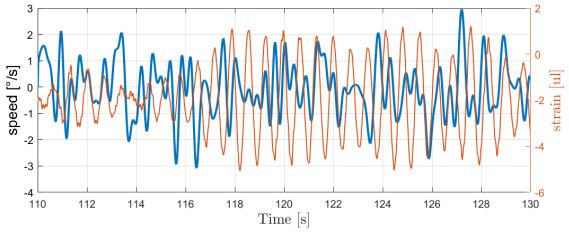

FIGURE 7. Multisine excitation signal assigned to joint 1 (blue) with the strain gauge response (orange).

application of flexible robotic platforms in various domains. However, as shown in Table 1, studies that incorporate higher degrees of freedom often exhibit other limitations, such as low/no payload and simple link structures.

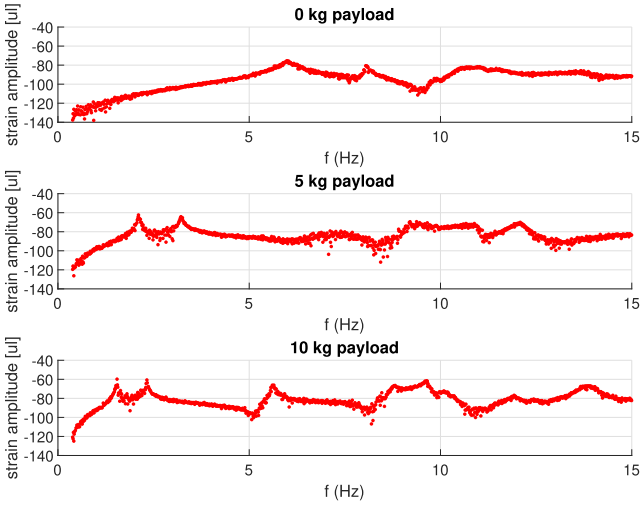

FIGURE 8. Example of frequency response function of the Best Linear Approximation of the parameter varying flexible manipulator. The influence of the different payloads is observed.

D. DIRECTION OF THE DEFLECTIONS

The direction of vibration in flexible link manipulators is dictated by the shape of the link and by the orientation of the actuator. The FLM setups described in the literature are designed to ensure that the vibrations of the links are perpendicular to the axis of rotation, while neglecting vibrations that occur parallel to it, as shown in Fig. 1 (top) [1], [4], [5]. However, researchers have conducted studies on the first fundamental frequencies, and their corresponding modes, of commercially available robots. Their findings

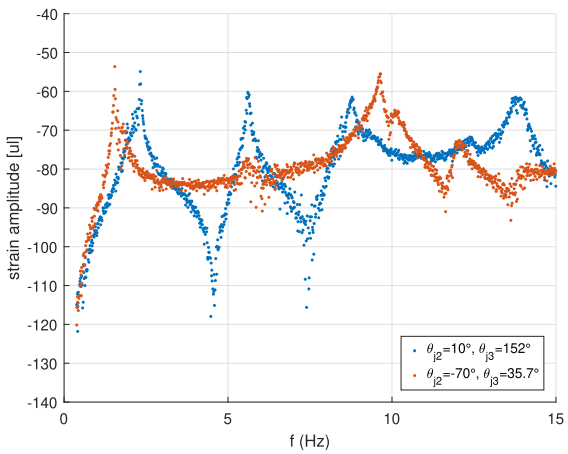

FIGURE 9. The Best Linear Approximation of the parameter varying flexible manipulator, showing the significance of varying joint angles. A constant payload of 10 kg was used.

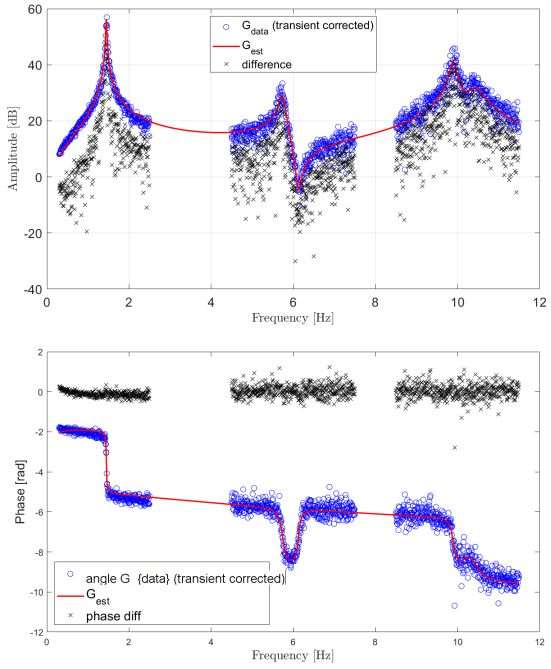

FIGURE 10. Estimated transfer function graphed in combination with the experimental response data (frequency domain) on the amplitude plot (top) and phase plot (bottom).

showed that the directions of the vibrations are parallel to the axis of rotation of the longest links, not perpendicular. Additionally, the base joint had the most critical influence regarding the dynamic behaviour [17], [18]. Fig. 1 (bottom) shows the direction of vibration parallel to the axis of rotation.

Therefore, this paper introduces a novel 3DOF flexible link manipulator tailored for industrial applications, featuring complex link shapes and designed to handle a high payload of 10 kg. Subsequently, a novel control strategy is developed to address the added complexities, which are often simplified,

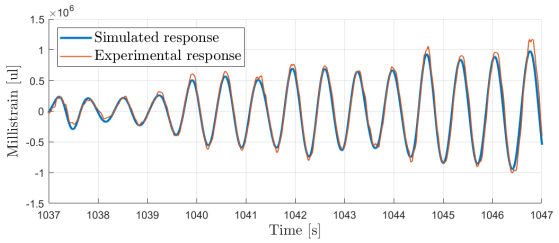

FIGURE 11. Section of the validation data of the estimated transfer function using a multisine trajectory of G_{FLM} for $\theta_{j2} = -90°$, $\theta_{j3} = 0°$ and $m_{pl} = 10$ kg.

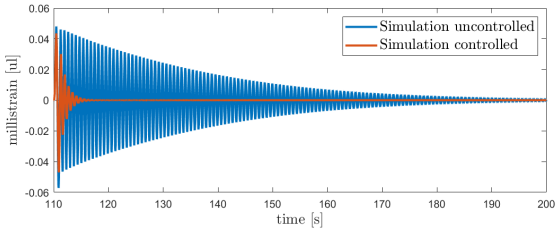

FIGURE 12. Simulation of the strain response, controlled vs. uncontrolled.

never combined, or treated separately in the literature. The FLM and its controller are evaluated based on the performance characteristics (such as repeatability, overshoot, settling time, peak torques, peak power, and energy consumption) for industrial applications. These characteristics are compared to those obtained for a rigid link manipulator (RLM) across experiments conform to industry standards. To do so, this paper uses an experimental setup where one flexible link manipulator and one rigid link manipulator are subjected to a series of experiments that reflect industry guidelines, specifications, requirements and applications. The outline of this paper is as follows; Section II and Section III describe the creation of the FLM and RLM and their control. Section IV and Section V describe the different experiments to evaluate both manipulators. During these experiments, the performance characteristics, such as repeatability, overshoot, settling time, peak torques, peak power and energy consumption are collected and discussed. The findings of the comparative analysis are summarized in the Conclusion, Section VI.

II. EXPERIMENTAL SETUPS

Two distinct experimental setups are created. The first setup involves a robot constructed with rigid links, which serves as the benchmark for comparison. The second setup features a robot designed with flexible links that are structurally robust enough to support both the payload of 10 kg and the robot's own mass. Both setups use the same actuators and are subjected to the same Denavit–Hartenberg parameters (DH-parameters), as seen in Table 2. The DH-parameters are based on the Kuka iiwa robots as this commercially available robot is a widespread robotic platform [7], [26], [27]. However, the degrees of freedom are limited to 3. Therefore, the DH-parameters for our design were calculated

TABLE 5. Repeatability of the FLM with vibration control (VC) and without vibration control (NVC). The repeatability of the rigid link manipulator and FLM VC are in close proximity and show similar repeatability.

	NVC [mm]	VC [mm]	rigid [mm]
0kg	0.105	0.022	0.018
5kg	0.491	0.030	0.030
10kg	2.069	0.138	0.0620

TABLE 6. Overshoot of the FLM with vibration control (VC) and without vibration control (NVC). Overshoot of the rigid link manipulator remains constant for different payloads showing very similar dynamics for a variety of payloads.

	NVC [mm]	VC [mm]	rigid [mm]
0kg	0.65	0.61	0.52
5kg	1.97	1.60	0.52
10kg	2.11	1.08	0.58

from the Kuka morphology, by only considering the base, shoulder and elbow joint of the Kuka as active joints, and considering the remaining joints as locked.

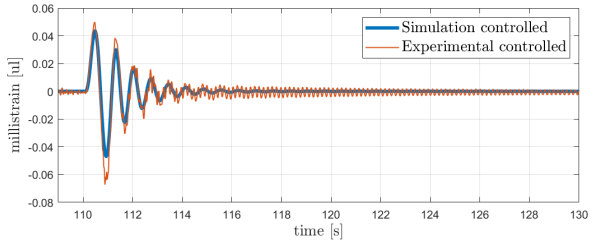

FIGURE 13. Simulation of the controlled strain response and the experimental data.

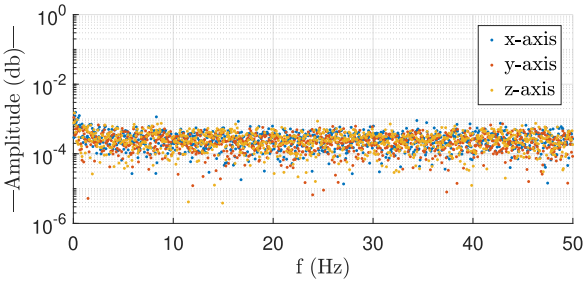

FIGURE 14. Static reference markers, which are mechanically separate from the robots, during test measurements show no noticeable influences such as external vibrations. Spectral analysis shows an equal energy distribution across all frequencies at a low level, ensuring precise measurements in x-,y- and z-axis. The noise represents deviations of the static reference markers in millimetres.

A. DESIGN OF THE FLEXIBLE LINKS

The loading conditions on the links are estimated such that the links can manipulate the payload of 10 kg, their own weight, and withstand inertial forces. F_x, F_y, F_z, M_x, M_y and M_z are calculated for every structural component for different θ, $\dot{\theta}$ and $\ddot{\theta}$. F_{xyz} and M_{xyz} are the forces and moments acting on the links in the reference frame of the joints for the

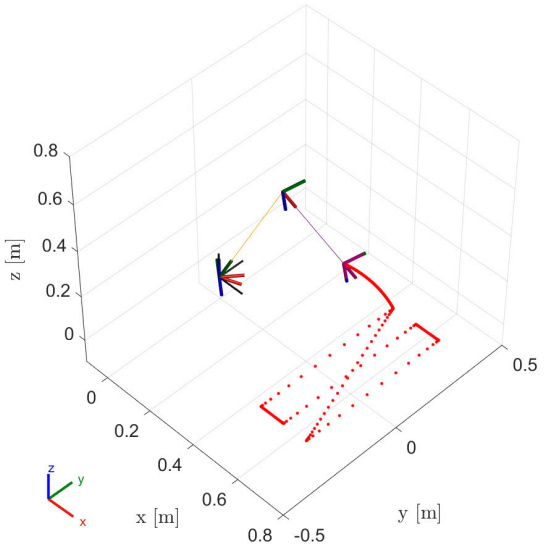

FIGURE 15. Trajectory of the repeatability experiment shown in Cartesian space. The trajectory includes a sequence from the home position to the start position, the trajectory itself, and a return sequence to the home position. Six individual points are reached sequentially, with a 7th-order polynomial trajectory used between each point for smooth transitions and minimal jerk.

TABLE 7. Settling time of the FLM with vibration control (VC) and without vibration control (NVC). The settling time of the FLM and NVC is not measurable according to the ISO norm as the vibrations do not have enough time to settle before the trajectory continues.

	NVC [s]	VC [s]	rigid [s]
0kg	0.09	0.06	0
5kg	not quantifiable	0.61	0
10kg	not quantifiable	0.87	0

x-, y- and z-direction, in Newton. θ, $\dot{\theta}$ and $\ddot{\theta}$ are the joint angles, joint speeds and joint accelerations respectively, in radians per second. From this dataset, the peak load cases are selected for further use in the design process. A safety factor (SF) of 1.25 is used to take into account unexpected forces such as the weight of cables, manufacturing tolerances and unequal mass distribution of the payload. The obtained forces are applied in a stress-constrained topology optimization. This results in a structure that is strong enough, as the stop-criteria is dependent on the stress levels inside the part, yet lightweight and inherently more flexible. This paper focuses on link 2 and link 3, as these links contribute the most to the moving mass and will create the largest amount of vibrations when they are optimized. Links 2 and 3 are shown in Fig. 2 by L_2 and L_3 respectively. The resulting robot has the properties described in table 3 and can be seen in Fig. 2.

B. ACTUATOR SELECTION

The actuator torque requirements are based on the same loading conditions of Section II-A. The speed of the actuator output are based on the joint speeds of the KUKA iiwa robot, which are between 75-85°/s. The selected actuators have the

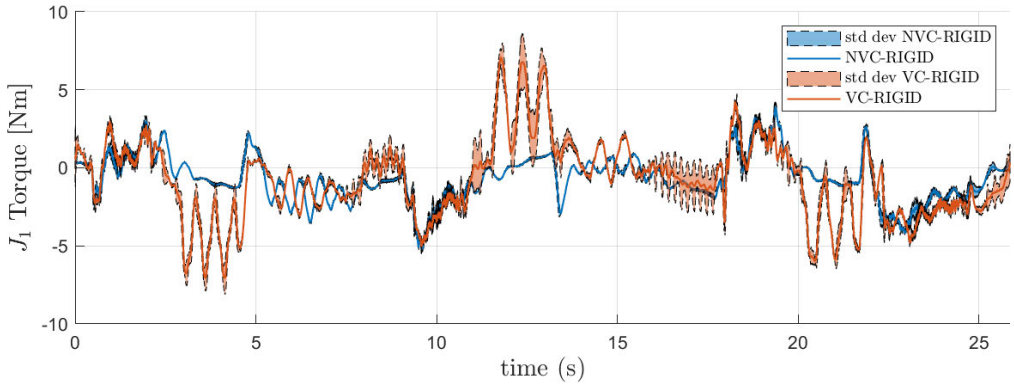

FIGURE 16. The torque differences and standard deviations for joint 1 of the flexible manipulators with vibration control (red) and without vibration control (blue), compared to those of the rigid manipulator for experiment 1 with a payload of 10kg. The vibration control results in significantly more oscillations (e.g. between 11s and 14s) in the torque to compensate for vibrations, which are not present when using the controller without vibration control.

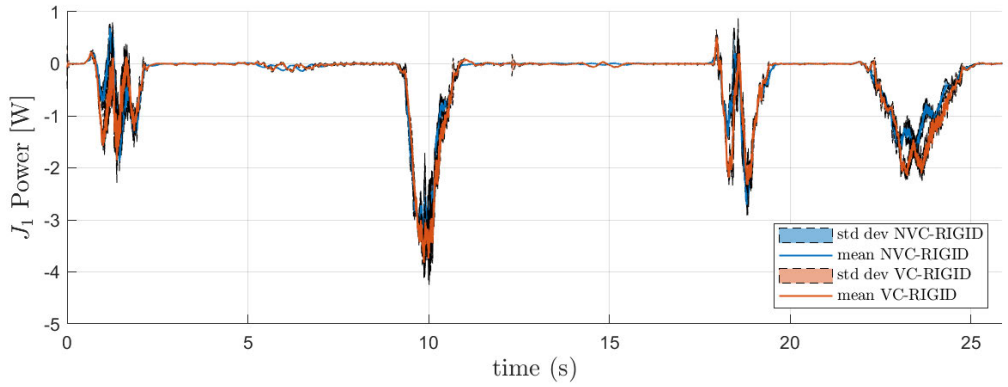

FIGURE 17. Power difference of joint 1 for flexible manipulators with vibration control (red) and without vibration control (blue), compared to the rigid manipulator for experiment 1 with a payload of 10kg. The peaks show that the major differences occur at the highest speeds of the trajectory.

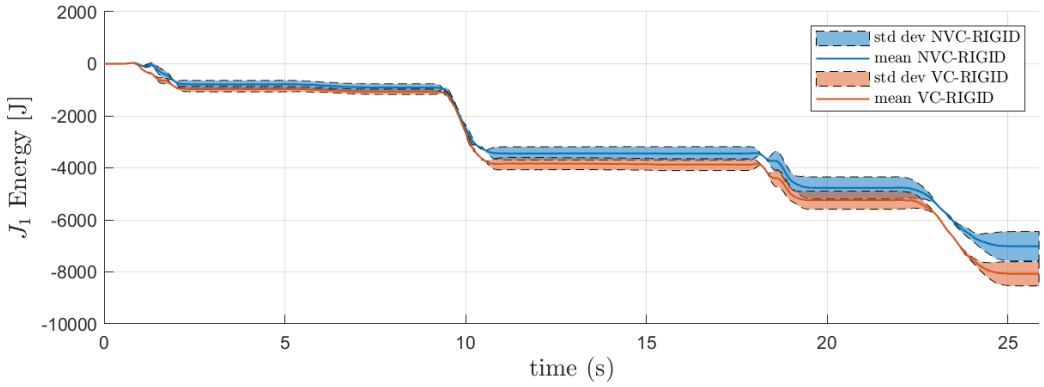

FIGURE 18. Energy difference and standard deviations of joint 1 of the flexible manipulators with vibration control (red) and without vibration control (blue), compared to the rigid manipulator for experiment 1 with a payload of 10kg. The flexible manipulator clearly shows a reduction of total energy consumption compared to the rigid manipulator wether vibration control is present or not. This indicates that the energy is lower due to the mass reduction of the flexible link manipulator.

controller, motor and gearbox integrated into one component, as is often the case with robots [27].

C. SENSING

Strain gauges are used to detect vibrations in flexible link manipulators. Strain gauges are highly sensitive to vibrations, offering precise measurements without being invasive. Their lightweight nature ensures that they do not add to or influence the dynamic vibrations of the flexible links, making them ideal for accurate and reliable vibration analysis in industrial applications. The link shape, derived from a stress-constrained topology optimization, results in a more uniform stress distribution compared to beams or cylinders [28]. This in turn means that the location of the

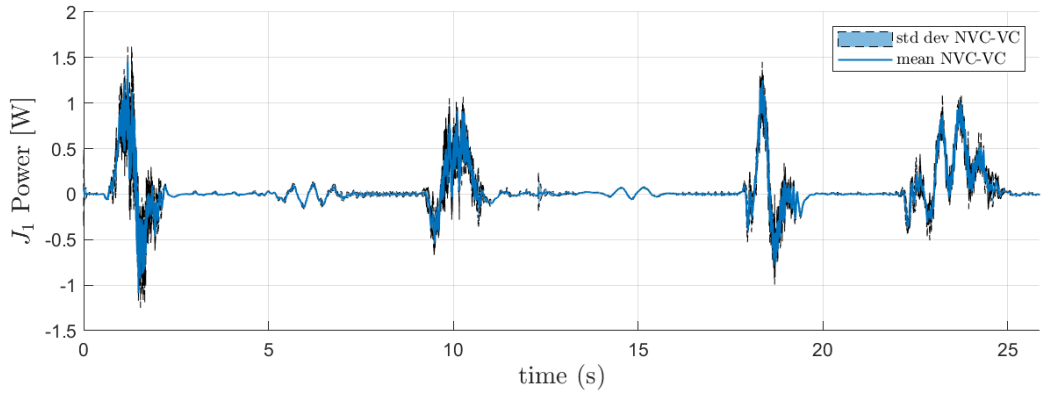

FIGURE 19. Power difference and standard deviations of joint 1 of the flexible manipulator with and without the vibration control for experiment 1 with a payload of 10kg. The peaks show that the major differences occur at the highest speed of the trajectory, as at these instances, the controller needs more power to compensate for the vibrations.

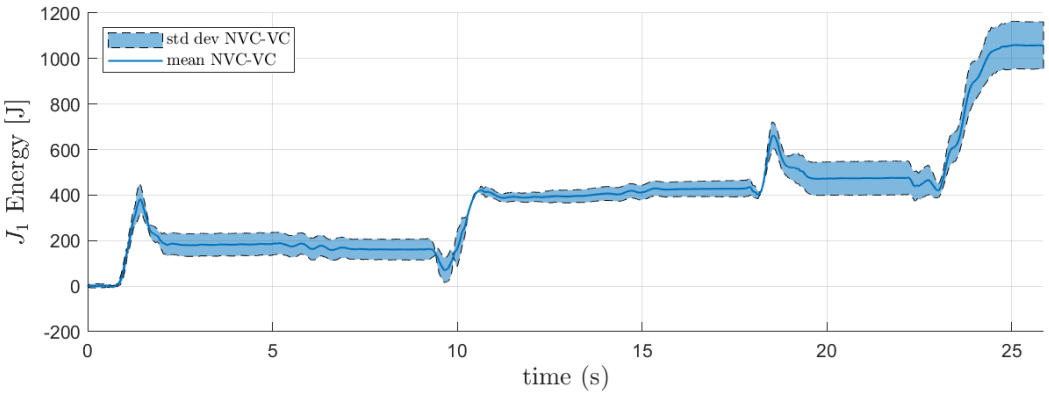

FIGURE 20. Energy consumption difference and standard deviations of joint 1 of the flexible manipulator with and without vibration control for experiment 1 with a payload of 10kg. More energy is required for the active vibration control. However, the energy saved from the usage of lighter flexible links is far greater than the added energy due to the vibration control.

strain gauges is less important. A Beckhoff system housed in an electrical cabinet together with power supplies and braking choppers is used for data acquisition (DAQ) and control [29].

D. DESIGN OF THE RIGID LINK SETUP

The setup with rigid link is created in a similar manner as described in Section II-A. The amount of deflection for every link is selected to be $\delta > 0.2\%$ of the length of the link for it to be considered a rigid link' [30]. To minimize variable differences, the same actuators are used in the rigid as with the flexible manipulator setups. However, the rigid robot is not equipped with strain gauges for vibration measurement, as its stiffness, similar to that of conventional robots, makes such measurements unnecessary. The resulting robot has the properties described in Table 3 and can be seen in Fig. 2.

TABLE 8. The root mean square (RMS) energy of the system's total energy consumption during Experiment 1, illustrating the energy usage across different payloads.

RMS Energy [J]	NVC	VC	RIGID
0kg	67435	67147	68735
5kg	72572	72748	74964
10kg	87200	87819	88599

TABLE 9. Maximum Torque of every joint given for the pick-and-place task with 10kg payload. Rigid manipulator has increased torques due to heavier links. Slight increase in joint 1 of vibration control compared to no vibration control due to the active strain feedback for vibration suppression.

Max Torque [Nm]	NVC	VC	Rigid
J1	18.65	18.84	18.86
J2	139.58	139.71	152.09
J3	128.40	128.07	129.92

III. CONTROLLER

The implementation of a controller is essential for vibration reduction in flexible link manipulators, as uncontrolled vibrations can severely compromise the robot's performance metrics. Without a properly designed controller, the inherent flexibility of the links can lead to significant oscillations, particularly during fast dynamic movements and/or when handling heavy payloads. These oscillations can cause inaccurate positioning, degraded task performance, and even

TABLE 10. Maximum Power of every joint given for the pick-and-place task with 10kg payload. Rigid manipulator has increased power due to heavier links. The maximum of the total trajectory is also given.

Max Power [W]	NVC	VC	Rigid
J1	18.40	20.11	19.22
J2	74.00	74.32	80.94
J3	63.19	62.95	63.09
Total	121.98	123.61	136.69

TABLE 11. RMS energy of every joint given for the pick-and-place task with 10kg payload. Rigid manipulator has increased power due to heavier links especially visible when looking at the total.

RMS energy [kJ]	NVC	VC	Rigid
J1	6.18	6.71	6.23
J2	32.79	32.83	36.94
J3	39.74	39.68	40.24
Total	66.82	65.97	71.95

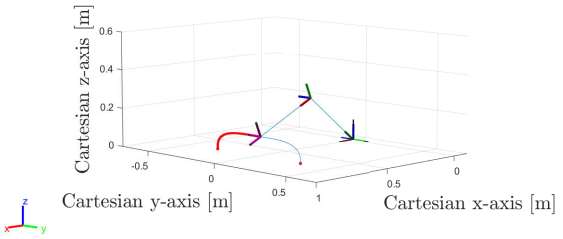

FIGURE 21. Pick-and-place task trajectory for a payload of 10 kg and end effector speed of 1.5 m/s.

potential damage to the system due to e.g. fatigue. Creating a controller for flexible link manipulators involves different steps and considerations compared to developing one for rigid link manipulators [4], [6]. The flowchart in Fig. 3 illustrates the extra steps necessary for controlling the flexible manipulator.

Before an adequate controller can be created for the flexible manipulator, more information about this flexible system is required. An experimental approach is used to identify the linear and non-linear dynamics and to what extent the payload and joint positions affect the robot dynamics. These 2 variables are explored for the following reasons.

Payload: The mass distribution between the robot and its payload can significantly influence the system's fundamental frequency, with an increase in payload leading to a reduction in the first fundamental frequency [23]. Additionally, the mass distribution influences the first fundamental frequency [23].

Joint Configurations: Similarly, variations in joint positions lead to alterations in the system's dynamic behaviour due to changes in mass distribution. Vieler demonstrated substantial shifts in both the range and direction of the fundamental frequency when joint positions were adjusted [18].

A. TUNING REGULAR JOINT CONTROLLERS

To ensure a meaningful comparison between the experimental setups of the flexible link manipulator and the rigid link manipulator, it is crucial that both control systems behave similarly on the joint level. This comparability allows us to attribute any observed differences in performance to the inherent characteristics of the manipulators themselves, rather than to discrepancies in the control strategies. By standardizing the control systems, reliable and valid data can be obtained that will facilitate a rigorous comparative analysis. Hence, before the identification of the FLM, a temporary regular velocity controller with an outer positional controller is used. In contrast to a position controller, the use of a velocity controller, combined with strain feedback control, can significantly enhance damping [25]. The controller used for the rigid-link manipulator is identical to that employed for the flexible-link manipulator, with the sole exception being the addition of the strain feedback, as discussed in Section III-G and shown in Fig. 5. In the case of the rigid-link manipulator, the strain feedback is disregarded, as it is not relevant to the system dynamics of a rigid structure. The two systems have been tuned to ensure that the controllers are robust enough to achieve identical dynamic responses on the joint level, even when operating at their maximum payload capacities. This tuning process involved optimizing the control parameters to maintain consistent performance metrics of the joint such as overshoot, position error, and settling time across both the flexible and rigid link manipulators. An example of a step response at high payloads can be seen in Fig. 4.

B. SYSTEM IDENTIFICATION

The first fundamental frequency is the most significant as it typically dominates the system's response. However, ignoring higher modes can lead to incomplete or inaccurate representations of behaviour, especially in complex systems [31]. Thus, during identification and modelling, higher modes are taken into account. A preliminary finite element analysis (FEA) and analytical estimations show the fundamental frequencies of the flexible link manipulator to be always higher than 1.5 Hz. Hence, to incorporate higher mode shapes, the identification will use a multisine, with a frequency range of 0.3-15 Hz and a frequency resolution of 0.005Hz, which is applied as an excitation to the base joint. This investigated frequency range is consistent with the fundamental frequencies of robots found in literature [18], [32]. Fig. 7 shows part of the excitation signal and the response during identification.

Nine periods of the multisine are applied to the first joint θ_{j1}, as this joint excites the vibrations the most. The first period is disregarded to avoid transient behaviour. Joint angles θ_{j2} and θ_{j3} are varied slowly during the experiment over a range of $-90°$ to $10°$ and $0°$ to $152°$ respectively, which includes most of the work envelope of the FLM. The corresponding response is measured using the strain

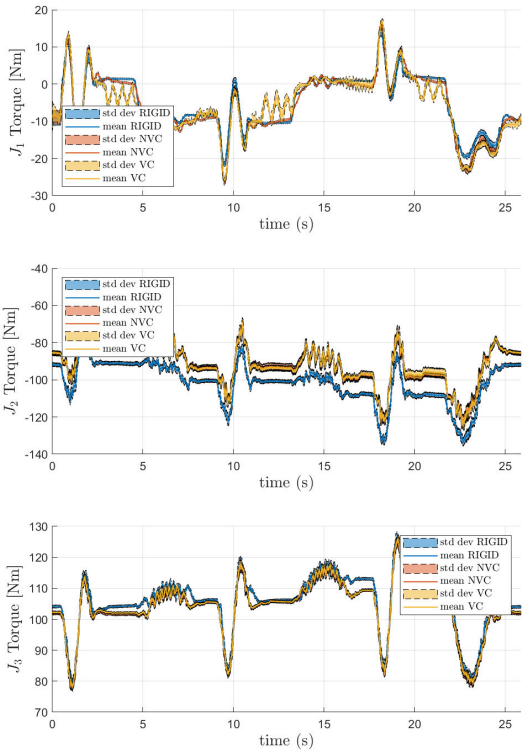

FIGURE 22. Joints torques for experiment 1 with a payload of 10kg.

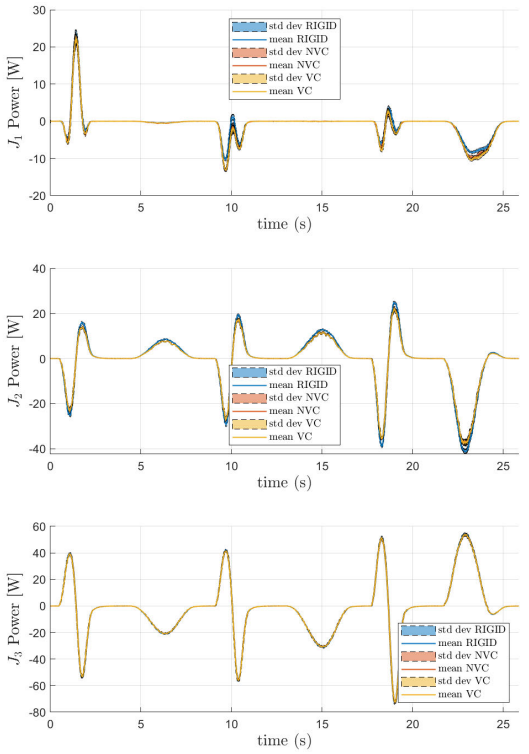

FIGURE 23. Joints mechanical power for experiment 1 with a payload of 10kg.

gauges at a sampling frequency of 1 kHz for each payload and for each position. The total experiment time for one identification multisine is approximately 26 minutes. The identification is repeated for different payloads, namely of 0, 5 and 10 kg and varying joint angles. Various identification trajectories are employed, each with slight variations. These variations include focusing on specific frequencies and using randomly distributed phases. This approach helps to capture a comprehensive range of system behaviours and responses.

During the identification process, it was observed, by using the Robust Method, that the nonlinearities of the FLM, indicated by the presence of odd, non-excited frequencies, are relatively minor compared to the varying system parameters like joint positions and payload changes [33, Section 4.3]. Therefore, the non-linearities are disregarded in the remainder of this paper. Fig. 8 shows the Best Linear Approximation (BLA) [33, Section 7.3] of the FLM for different payloads, showing the influence of a varying payload. Here, the reduction of the fundamental frequency becomes apparent with increasing payload. Similarly, Fig. 9 shows the influence of the joint positions on the dynamic response for a payload of 10kg. This highlights the necessity of using a controller that can adapt to payload changes and joint variations to cancel vibrations effectively.

C. EDGE CASE IDENTIFICATION

So far, this paper has focused on the initial identification of the system, aiming to find its dominant behaviours, which are the joint positions and the payload. Additionally, it has provided insights into the complexity of the system dynamics, highlighting that modelling and predicting vibrations using traditional models, such as assumed modes method, finite elements method and lumped parameter modelling, is impractical for real-time control. This is due to factors such as complex link structures, uneven mass distribution, a high number of degrees of freedom, and the direction of the vibrations, which are reliant on computationally intense modelling techniques [3]. Therefore, a data-driven approach is employed instead. In order for accurate modelling and tuning, more identification is done with a focus on static edge cases of the robots work envelope. The edge cases represent the extremes of the system's operating conditions, specifically based on the fundamental frequency. By designing gains for these points, we ensure that the controller can handle the entire range of system behavior. By designing for edge cases, we effectively bound the worst-case performance. Instead of designing gains for every possible operating point (which is infeasible), this paper chooses a finite set of representative points making the design process more tractable. The edge cases are selected based on the positions where the robots' first fundamental frequency changes from minimum to maximum for a given payload. This method is also consistent with the work of Vieler et al., who investigated the first fundamental frequency in relation to the end effector position within the work

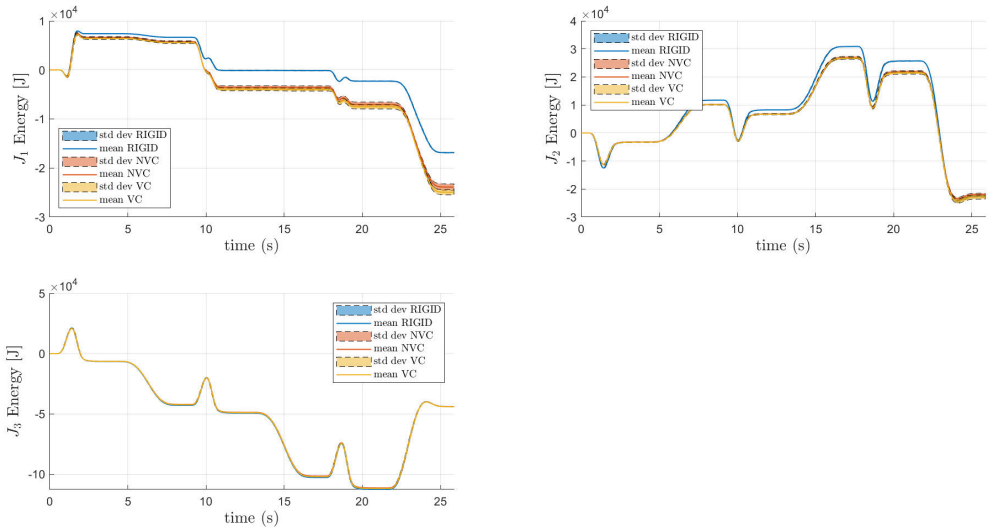

FIGURE 24. Joints energy for experiment 1 with a payload of 10kg.

envelope of a rigid manipulator, showing results similar to our system identification findings [18]. This approach ensures that only interpolation of the control parameters is necessary, avoiding the potential errors associated with extrapolation. More information on the control parameters can be found in Section III-G. This approach is illustrated with an example to show how it was used to tune the controller effectively. Data from the identification process in section III-B is used to select intermediate points of the flexible link manipulator. This edge case example will focus on one of its most challenging configurations: fully horizontally stretched out with a high payload, $\theta_{j2} = -90°$, $\theta_{j3} = 0°$ and $m_{pl} = 10$ kg. This configuration is most prone for vibrations in the horizontal plane, and can only be countered using the base joint. This configuration has a minimum of 1.55 Hz. Additional identification trajectories are applied, similarly as described in Section III-B. The data gathered is used to create an edge case model. The bode plot and estimated transfer function of this example is visible in Fig. 10 and the fundamental frequencies and their respective damping ratios can be found in table 4.

D. EDGE CASE MODELING

A transfer function is used to determine the input/output (motion induced by joint velocity / strain) relationship, represented by G_{FLM} in Fig. 5. The transfer function is estimated via a Maximum Likelihood approach in the frequency domain, as outlined in [33, Section 9.11]. The estimated transfer function, plotted in Figure 10, is given by:

$$G(s) = \frac{\sum_{n=0}^{7} b_n s^n}{\sum_{n=0}^{8} a_n s^n} \tag{1}$$

E. MODEL VALIDATION

The predicted input-output of the reduced-order model is validated against additional experiments, visible in Fig. 11.

F. EDGE CASE TUNING

Once the transfer function is estimated and validated, it can be utilized to fine-tune one of the edge cases of the adaptive controller. The goal of this tuning process is to achieve the shortest possible settling time. For the specific scenario when $\theta_{j2} = -90°$, $\theta_{j3} = 0°$ and $m_{pl} = 10$ kg, a significant reduction of 94% in settling time was achieved, as illustrated in Fig. 12 and Fig. 13.

This summarizes the process of tuning the adaptive control for one of the edge cases. Various edge cases were examined, each involving different combinations of payloads and joint positions.

G. CREATION OF ADAPTIVE CONTROLLER

The different edge cases that were investigated were combined to create a lookup table for the gain scheduler of the adaptive controller. The gain scheduler was constructed, utilizing linear interpolation between all the explored cases. While much of this process was automated using MATLAB, it still requires a significant amount of manual processing. The time invested in identifying, modelling and tuning of the cases will dictate the effectiveness of the controller tuning. The more edge cases and intermediate cases that are explored, the better the controller can be tuned. The overall control schematic of the FLM can be seen in Fig. 5 and the adaptive controller can be seen in Fig. 6.

H. EXPERIMENTS

Two distinct experiments are conducted. The first experiment quantitatively assesses the performance of both manipulators based on the ISO 9283 norm. The second experiment involves a pick-and-place task, evaluating the manipulators's performance based on its ability to successfully complete the task and look at the maximum torques, power and energy consumption.

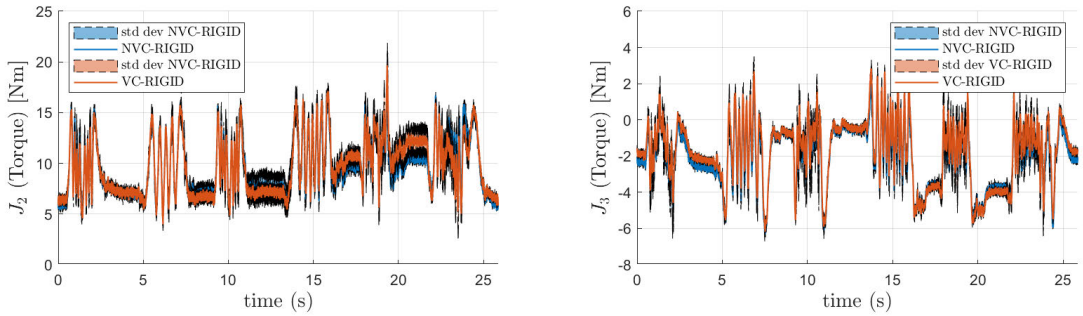

FIGURE 25. The torque differences and standard deviations for joints 2 and 3 of the flexible manipulators with vibration control (red) are compared to those of the rigid manipulator for experiment 1 with a payload of 10kg. Similarly, the torque differences and standard deviations for joints 2 and 3 of the flexible manipulators without vibration control (blue) are compared to the rigid manipulator for experiment 1 with a payload of 10kg. A reduction of 20 Nm is observed for a 10 kg payload in joint 2, demonstrating the advantages of lightweight flexible links. This suggests that smaller actuators with lower torque requirements could potentially be used when flexible links are implemented. Similarly, lower torques can be expected in joint3. No major differences are visible between the FLM with and without vibration control as the vibration control has no effect on these joints.

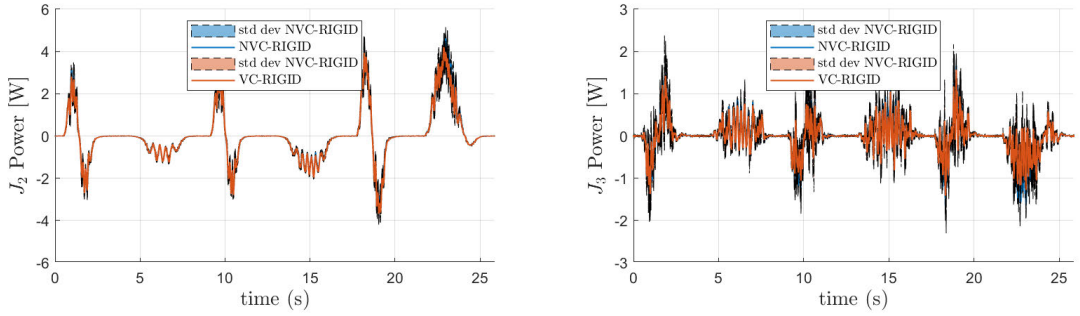

FIGURE 26. Power difference of joints 2 and 3 for flexible manipulators with vibration control (red) compared to the rigid manipulator for experiment 1 with a payload of 10kg. Power difference of joints 2 and 3 for flexible manipulators without vibration control (blue) compared to the rigid manipulator for experiment 1 with a payload of 10kg. The flexible manipulator demonstrates a reduction in power for up to 300W in some instances. No major differences are visible between the FLM with and without vibration control as the vibration control has no effect on these joints.

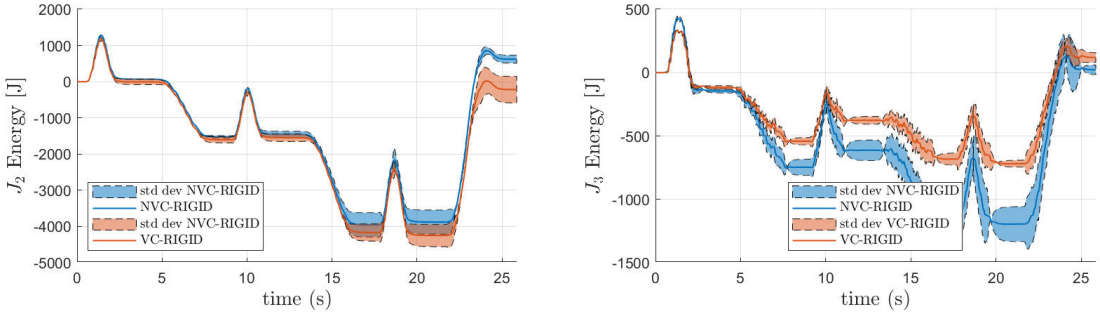

FIGURE 27. Energy difference and standard deviations of joints 2 and 3 of the flexible manipulators with vibration control (red) compared to the rigid manipulator. Energy difference and standard deviations of joints 2 and 3 of the flexible manipulators without vibration control (blue) compared to the rigid manipulator. No major differences are visible between the FLM with and without vibration control as the vibration control has no effect on these joints.

All experiments are performed in a temperature-controlled room, with no people present in the measurement environment [34]. In addition, following the manufacturer's guidelines, the measurement equipment is powered on one hour prior to the beginning of the measurements, to allow for thermal equilibrium of the measurements' sensors. Once thermal equilibrium is achieved, the optical measurement system is calibrated. In addition, the robots are painted mate black to avoid reflections which can cause the optical measurement system to be inaccurate, as can be seen in Figure 2.

Measures to avoid environmental influences are implemented at various levels. Firstly, only shielded cables are used for robot control and data acquisition. Additionally, special

shielding tape is applied to the strain gauges's leads to prevent any environmental electrical contamination of the signal used for the controller. Secondly, independent reference markers are used to verify the presence of environmental influences such as ground vibrations. Figure 14 illustrates the results of spectral analysis of one of the reference markers, demonstrating an equal energy distribution across all frequencies at a sufficiently low level to ensure precise measurements in x-,y- and z-axis. Thus, showing that the deviations measured are considered to be noise only. The noise represents the deviations of the static reference markers in millimetres.

IV. EXPERIMENT 1: ASSESSMENT OF THE REPEATABILITY

ISO 9283 outlines the methods for measuring and evaluating the performance of industrial robots, particularly focusing on their accuracy, repeatability, and other operational characteristics. The purpose of ISO 9283 is to provide a consistent framework for assessing these performance metrics, enabling manufacturers and users to compare different robots objectively [34]. The key performance characteristic in industry is 'repeatability', this is the only metric that is consistently shared by robotic manufacturers. However, more performance characteristics will be used and compared in this experiment. To assess repeatability, the robot is programmed to follow a trajectory defined by the ISO 9283 standard. The trajectory, shown in Figure 15, includes a sequence from the home position to the start position, the trajectory itself, and a return sequence to the home position. Six individual points are reached sequentially, with a 7th-order polynomial trajectory used between each point for smooth transitions and minimal jerk. Figures 30 and 31 show one period of the trajectory for this experiment in joint space. These tests are conducted with a payload of 0, 5 and 10 kg and an end effector speed of up to 1.5 m/s. This end effector speed is higher than the typical end effector speed of around 1 m/s, for industrial robots and 0.25 m/s for collaborative robots, to account for highly dynamic conditions [35], [36], [37], [38]. Joint speeds and accelerations reach up to 1.33 rad/s and 2.83 rad/s^2, respectively. The trajectories are performed while the end effector position is measured, such that the repeatability can be determined as:

$$R_p = \max R_{pi} = \max \left[\bar{l}_i + 3S_{li}\right] \quad i = 1 \ldots m \tag{2}$$

The repeatability R_p is the maximum R_{pi} which represents the radius of a circle in the normal plane and with its centre on the barycentre line of the trajectory [34]. Where i is the indicator of what trajectory is performed and where $m = 3$, which is the total number of trajectories performed. And $\bar{l}_i$ is the mean of the repeated paths formulated as:

$$\bar{l}_i = \frac{1}{n}\sum_{j=1}^{n} l_{ij} \tag{3}$$

Here is $j = 10$, which is the number of times the i^{th} trajectory has been performed a number of j-times, and is a requirement of the ISO 9283 norm. The standard deviation of the trajectory S_{li}, can be written as:

$$S_{li} = \sqrt{\frac{\sum_{j=1}^{n}\left(l_{ij} - \bar{l}_i\right)^2}{n-1}} \tag{4}$$

And l_{ij} can be written as:

$$l_{ij} = \sqrt{\left(x_{ij} - \bar{x}_i\right)^2 + \left(y_{ij} - \bar{y}_i\right)^2 + \left(z_{ij} - \bar{z}_i\right)^2} \tag{5}$$

x_{ij}, y_{ij} and z_{ij} are the measured spacial positions for the i^{th} trajectory of the j^{th} path for the x, y and z coordinates respectively, in cartesian space. $\bar{x}_i$, $\bar{y}_i$ and $\bar{z}_i$ are the mean values of the i^{th} trajectory, giving a barycentre line of all j-amounts of paths taken. The data collected from these cycles is then analysed to determine the repeatability of the systems.

The results of the experiments are displayed in Tables 5-7 showing the repeatability, the overshoot and the settling time.

The repeatability of a RLM is dependent on the payload [36]. This is confirmed by the results in Table 5 for a FLM, with an increase in payload, so does the repeatability increase. Typical RLMs/commercially available robots have a repeatability ranging from 0.4 mm to 0.02 mm. From the experimental results, it is clear that the FLM without vibration control is performing significantly worse compared to commercially available robots when there is no vibration control. However, when vibration control is applied, the repeatability falls within the range of commercial robots. The repeatability tests demonstrated that the flexible manipulator achieved a repeatability of 0.138 mm at a 10 kg payload. This level of repeatability is comparable to that of traditional rigid manipulators. These results indicate that a flexible link manipulator, even with these complex link structures and high payload capacity, can perform on par with commercially available rigid robots when equipped with an advanced control system. This finding underlines the potential of flexible link manipulators to match the performance standards of rigid robots in industrial applications.

However, repeatability should not be the only performance factor. Overshoot and settling time should also be considered, especially with flexible manipulators.

Overshoot is calculated as:

$$O = \max O_j \tag{6}$$

And O_j is the overshoot for different trajectories and can be expressed as:

$$\begin{aligned} O_j &= \max D_{ij} \quad if \ \max D_{ij} > limit\ band \\ &= 0 \quad if \ \max D_{ij} \leqslant limit\ band \end{aligned} \tag{7}$$

Here, D_{ij} represents the overtravel distance of the robots end effector compared to the barycentre of the measured point for the ith trajectory of the jth path. The limit band in this formulation represents the repeatability. Settling time is related to the overshoot as it is the time necessary for a robot to stabilize at the attained pose.

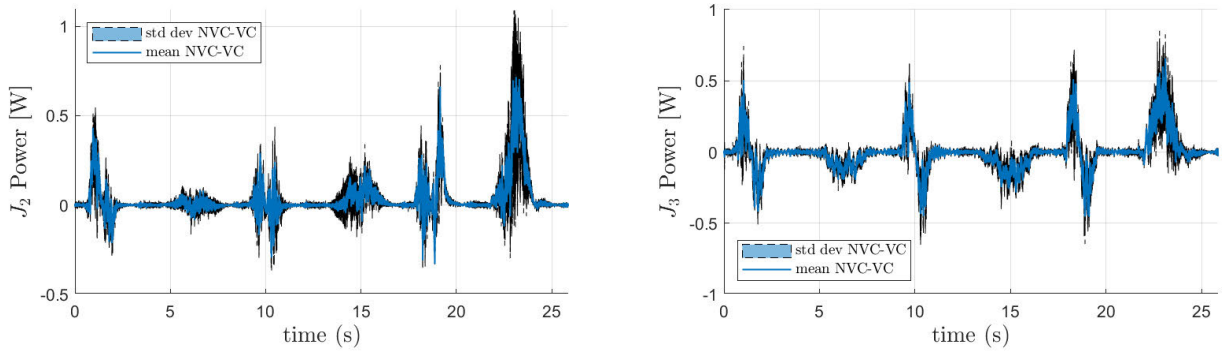

FIGURE 28. Power difference and standard deviations of joint 2 and 3 of the flexible manipulator with the vibration control compared to without vibration control for experiment 1 with a payload of 10kg.

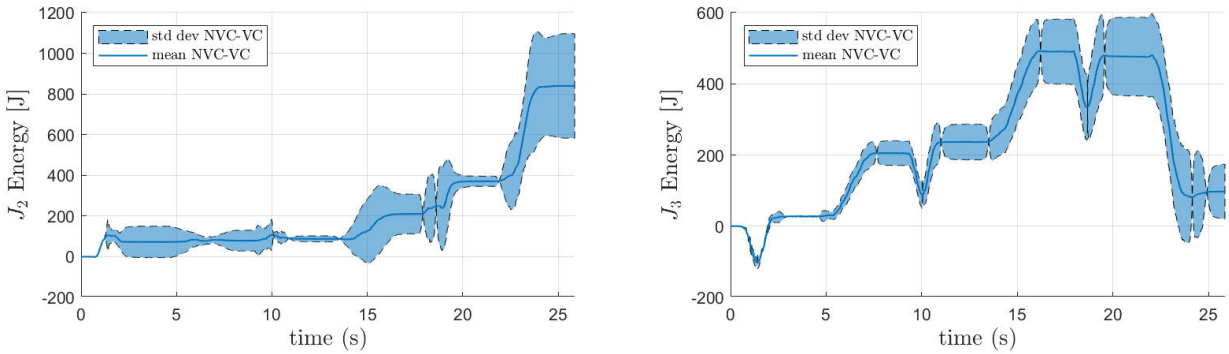

FIGURE 29. Energy consumption difference and standard deviations of joint2 and 3 of the flexible manipulator with the vibration control compared to without vibration control for experiment 1 with a payload of 10kg.

The flexible link manipulator exhibits relatively high overshoot and settling time compared to the rigid manipulator, as can be seen in Table 6 and Table 7. Depending on the specific task, these performance metrics might be excessive and could impact the suitability of the flexible manipulator for certain applications. It is important to note that the comparison of overshoot and settling time is challenging because manufacturers do not provide these metrics for their robots and especially as it is highly dependent on the control strategy. This lack of standardised data makes it difficult to directly compare and position the performance of flexible and rigid manipulators based on these criteria. Overshoot and settling time can be reduced by fine-tuning the parameters of the adaptive controller. However, this adjustment is likely to come with trade-offs. Specifically, improving these metrics may result in increased cycle times and reduced operational speeds. Another strategy is to simply reduce the manipulator's operating speed. In certain applications, such as collaborative robot, speed is intentionally limited. This reduction in speed leads to less dynamic excitation, making it easier to manage vibrations and improve overall system stability. Table 6 and Table 7 both show that vibration control is necessary for better performance of an FLM. The settling time of a flexible structure without vibration control is so high that it is considered 'not quantifiable' according to the ISO 9283 standard.

Additionally, in Table 6, the FLM with VC exhibits a higher overshoot at a payload of 5kg compared to a payload of 10kg, indicating poorer performance at the lower payload. This observation is not counterintuitive, as the relationship between overshoot and payload is not expected to be linear nor expected to be always increasing with increasing payload. Similar to the findings for rigid manipulators by Offodile et al., it was also demonstrated that repeatability does not consistently increase with increasing payload or speed, but it also shows there are combinations of lower speeds and lower payloads that yield worse repeatability values [36]. To address this behaviour, one potential solution is to fine-tune the adaptive controller for specific scenarios involving lower payloads. Instead of using a general approach as shown in Fig. 3, it would be beneficial to customise the controller for particular tasks where the payload and trajectories are predetermined. This targeted tuning could enhance the controller's performance by accounting for the unique dynamics and requirements of each specific situation, leading to more precise and reliable operation under varying conditions. Notably, when no payload is present, the flexible links behave very much like a rigid link.

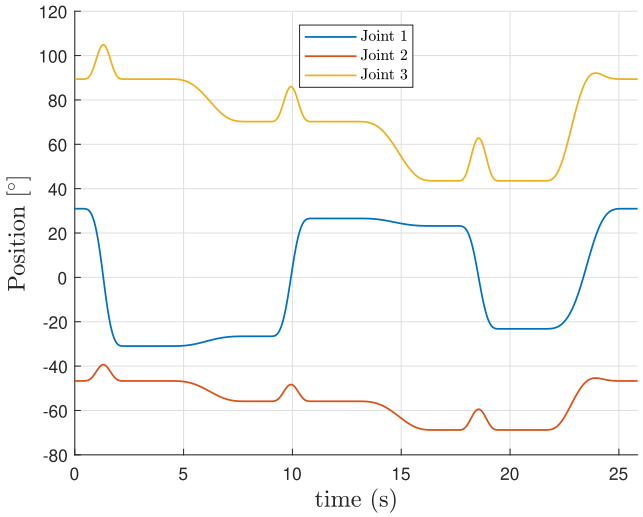

FIGURE 30. Joint positions of one period of the path taken for repeatability tests in degrees.

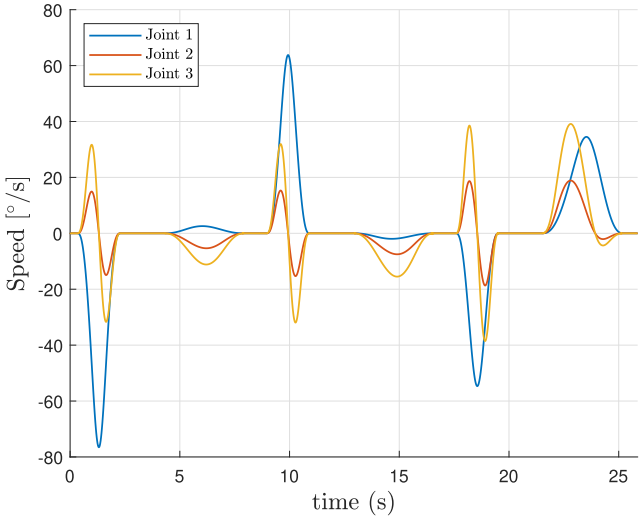

FIGURE 31. Joint speeds of one period of the path taken for repeatability tests in degrees.

One of the main advantages of flexible links is their reduced mass, which can significantly impact joint torques, power requirements, and energy consumption in robotic tasks. Since there is no definitive consensus in the literature on which trajectories or tasks to use for investigating these performance characteristics, this paper will utilize the trajectories provided by the ISO 9283 norm. Although ISO 9283 is primarily used for repeatability assessment, its trajectories can also be effectively used for analyzing power and energy consumption. Figures 16-18 respectively show the obtained torque, power and energy values obtained for this trajectory. To enhance interpretation of the results, the results obtained with and without vibration control are shown as difference with respect to the values obtained for the rigid link robot. Figure 16 shows the mean values and the standard deviation of the torques of joint 1. Additional torque oscillations can be seen when the vibration suppression is active.

Figure 17 presents a comparison of the power differences between the rigid manipulator and the flexible link manipulators (with and without vibration control). The mean values and standard deviation of the power of joint 1 is calculated as:

$$P_{ij,J1} = \tau_{ij,J1}\omega_{ij,J1} \tag{8}$$

$$\bar{P}_{i,J1} = \frac{1}{n}\sum_{j=1}^{n} P_{ij,J1} \tag{9}$$

$$P_{i,J1\,std\,dev} = \sqrt{\frac{\sum_{j=1}^{n}\left(P_{ij,J1} - \bar{P}_{i,J1}\right)^2}{n-1}} \tag{10}$$

Figure 17 illustrates that for a 10kg payload, mechanical power consumption of joint 1 can be reduced by up to 4.1W at a given moment, which is significant when considering that the maximum power of the initial power requirement is 24W, visible in Figure 23. Similar findings for joints 2 and 3 can be seen in Figure 28 , indicating that the FLM required less power. When examining Figure 17, it was anticipated that the torque oscillations between 11s and 14s from Figure 16 would also be present in the power. However, due to the low speed required to minimize the vibrations, the power is negligible compared to the power reduction of the payload to move at high speed. In this case, the mass reduction of the structure is the dominant factor. This reduction is also reflected in the total energy consumption, as shown in Figure 18 by the mean values of the path and the standard deviation, indicating that flexible manipulators can save overall energy regardless of whether vibration control is active. This can also be seen for joints 2 and 3 in the Appendix, Figure 29. The energy consumption $E_{ij,J1}$ for a given trajectory and path for joint 1 is calculated as:

$$E_{ij,J1} = \int^{t} P_{ij,J1}dt \tag{11}$$

And the mean energy for the trajectory after performing the path a j-number of times for joint 1, which is the energy used to make the comparisons in Figures 16-20:

$$\bar{E}_{i,J1} = \int^{t} \bar{P}_{i,J1}dt \tag{12}$$

With the standard deviation:

$$E_{i,J1\,std\,dev} = \sqrt{\frac{\sum_{j=1}^{n}\left(E_{ij,J1} - \bar{E}_{i,J1}\right)^2}{n-1}} \tag{13}$$

As introduced above, FLMs need active vibration compensation to obtain better performance characteristics, which in turn increases the energy consumption. Figures 19-20 show how much additional power and energy is required for vibration control to compensate the vibrations, calculated using Equation 8-11. From this this paper demonstrates that the energy saved from the usage of lighter flexible links is far greater than the added energy due to the vibration control.

The analysis of power and energy consumption primarily focused on joint 1, as it is the joint responsible for reducing vibrations. Detailed graphs for all joints can be found in Appendix. Furthermore, the total RMS energy of the manipulators can be found in Table 8 for every payload.

V. EXPERIMENT 2: PERFORMANCE EXPERIMENT

An additional pick-and-place task (PAP) is selected for evaluating the robot's performance due to its fundamental and broadly applicable nature. Pick-and-place operations are straightforward and represent basic functionalities that are present in numerous industrial applications. This simplicity allows for a clear assessment of essential performance characteristics, energy consumption, peak power, etc. without the added complexity of more intricate tasks [39]. The trajectory of the PAP task can be seen in Fig. 21.

The results of the experiments are displayed in Tables 9-11 showing the peak torques, peak power and energy consumption for a PAP task of 10kg.

Tables 9-11 illustrate the considerable advantages of utilizing lightweight flexible links. One of the most notable improvements is the significant reduction in energy consumption for a 10kg pick-and-place task. Although more energy is put into the system to actively dampen vibrations with joint 1, the overall energy consumption remains lower compared to that of a rigid manipulator. This efficiency gain highlights the potential for flexible link manipulators to operate more sustainably and cost-effectively. Additionally, when comparing the rigid manipulator to the flexible link manipulator, a notable reduction in maximum torque and power requirements is evident, particularly in joints 2 and 3. The use of flexible links allows for a reduction in actuator requirements. By needing smaller and less powerful actuators, the overall system can benefit from lower weight actuators and lower operating cost.

VI. CONCLUSION

This paper demonstrates advantages and arguments for flexible link manipulators that can be realized without the restrictive assumptions commonly found in the literature. These assumptions typically include low payload capacity, limited degrees of freedom, simplified link structures, and vibrations parallel to the axis of rotation. This paper presents the development and comparison of a flexible link manipulator without these restrictive assumptions and a rigid manipulator. Both experimental setups are evaluated against each other, with their performance measured and analyzed. The results demonstrate that flexible link manipulators can be designed and utilized in a reliable manner, making them suitable for real-world applications. Specifically, the repeatability of the flexible link manipulator of 0.138 mm is shown to be comparable to that of commercially available rigid robots, making flexible link manipulators much more suitable for real-world applications than originally anticipated. While we have demonstrated that flexible link manipulators (FLMs) can achieve repeatability on par with commercially available rigid link manipulators, other performance metrics, such as overshoot and settling time, suggest that FLMs are better suited for applications involving lower dynamic loads or slower operational speeds. Operating under these conditions helps mitigate the effects of overshoot and reduces settling time, thereby enhancing overall control stability. One example of such an application may be collaborative robots. Collaborative robots function at reduced speeds and the reduced mass of the flexible link manipulators make them safer compared to the rigid link manipulators. However, it is important to note that evaluating the suitability of flexible link manipulators for collaborative tasks was beyond the scope of this study. Future investigations should explore this potential more thoroughly, particularly in terms of safety certification, human-robot interaction dynamics, and compliance with collaborative robotics standards.

Additionally, energy consumption of a flexible link manipulator is lower compared to a rigid manipulator even with active vibration suppression. Future work will focus on the development of safe interaction controllers, along with conducting impact tests to gain a deeper understanding of flexible manipulators in collaborative environments. A key focus will be on improving safety to ensure reliable and secure interactions between humans and robots. Additionally, we plan to incorporate a wrist mechanism, adding an extra 3 degrees of freedom (3DOF), to further enhance the manipulator's capabilities.

APPENDIX A
REPEATABILITY TRAJECTORY 10KG

APPENDIX B
JOINT 2 AND JOINT 3 PERFORMANCE CHARACTERISTICS

ACKNOWLEDGMENT

The authors would like to thank Tom Turcksin for his assistance in conducting the experiments at the AugmentX Research Laboratory. They would like to thank Marnix De Boom and Jeroen De Turck for their help with manufacturing parts.

REFERENCES

[1] M. Sayahkarajy, Z. Mohamed, and A. A. M. Faudzi, "Review of modelling and control of flexible-link manipulators," *Proc. Inst. Mech. Eng., I, J. Syst. Control Eng.*, vol. 230, no. 8, pp. 861–873, Sep. 2016, doi: 10.1177/0959651816642099.

[2] S. K. Dwivedy and P. Eberhard, "Dynamic analysis of flexible manipulators, a literature review," *Mechanism Mach. Theory*, vol. 41, no. 7, pp. 749–777, Jul. 2006. [Online]. Available: https://www.sciencedirect.com/science/article/pii/S0094114X06000292

[3] B. Li, X. Li, H. Gao, and F.-Y. Wang, "Advances in flexible robotic manipulator systems—Part I: Overview and dynamics modeling methods," *IEEE/ASME Trans. Mechatronics*, vol. 29, no. 2, pp. 1100–1110, Apr. 2024.

[4] B. Li, X. Li, H. Gao, and F. Wang, "Advances in flexible robotic manipulator systems—Part II: Planning, control, applications, and perspectives," *IEEE/ASME Trans. Mechatronics*, vol. 29, no. 3, pp. 1680–1689, Jun. 2024.

[5] D. Subedi, I. Tyapin, and G. Hovland, "Review on modeling and control of flexible link manipulators," *Model., Identificat. Control, Norwegian Res. Bull.*, vol. 41, no. 3, pp. 141–163, 2020.

[6] K. Lochan, B. K. Roy, and B. Subudhi, "A review on two-link flexible manipulators," *Annu. Rev. Control*, vol. 42, pp. 346–367, Dec. 2016. [Online]. Available: https://www.sciencedirect.com/science/article/pii/S1367578816300736
[7] G. Van de Perre, T. Hubert, T. Verstraten, and B. Vanderborght, "Investigating the potential of flexible links for increased payload to mass ratios for collaborative robotics," *IEEE Access*, vol. 11, pp. 15981–15995, 2023.
[8] W. He, H. Gao, C. Zhou, C. Yang, and Z. Li, "Reinforcement learning control of a flexible two-link manipulator: An experimental investigation," *IEEE Trans. Syst., Man, Cybern., Syst.*, vol. 51, no. 12, pp. 7326–7336, Dec. 2021.
[9] M. Sasaki, J. Muguro, W. Njeri, and A. S. A. Doss, "Adaptive notch filter in a two-link flexible manipulator for the compensation of vibration and gravity-induced distortion," *Vibration*, vol. 6, no. 1, pp. 286–302, Mar. 2023.
[10] M. Shao, Y. Huang, and V. V. Silberschmidt, "Intelligent manipulator with flexible link and joint: Modeling and vibration control," *Shock Vib.*, vol. 2020, pp. 1–15, Jan. 2020.
[11] L. Tang, M. Gouttefarde, H. Sun, L. Yin, and C. Zhou, "Dynamic modelling and vibration suppression of a single-link flexible manipulator with two cables," *Mechanism Mach. Theory*, vol. 162, Aug. 2021, Art. no. 104347.
[12] Q. Meng, X. Lai, Z. Yan, C.-Y. Su, and M. Wu, "Motion planning and adaptive neural tracking control of an uncertain two-link Rigid–Flexible manipulator with vibration amplitude constraint," *IEEE Trans. Neural Netw. Learn. Syst.*, vol. 33, no. 8, pp. 3814–3828, Aug. 2022.
[13] M. Sasaki, J. Muguro, F. Kitano, W. Njeri, D. Maeno, and K. Matsushita, "Vibration and position control of a two-link flexible manipulator using reinforcement learning," *Machines*, vol. 11, no. 7, p. 754, Jul. 2023. [Online]. Available: https://www.mdpi.com/-1702/11/7/754
[14] P. Sarkhel, M. K. Dikshit, V. K. Pathak, K. K. Saxena, C. Prakash, and D. Buddhi, "Robust deflection control and analysis of a fishing rod-type flexible robotic manipulator for collaborative robotics," *Robot. Auto. Syst.*, vol. 159, Jan. 2023, Art. no. 104293.
[15] J. Malzahn, "Modeling and control of multi-elastic-link robots under gravity: From oscillation damping and position control to physical interaction," Ph.D. dissertation, Faculty Elect. Eng. Inf. Technol., Technische Universität, Berlin, Germany, 2014.
[16] J. K. Viswanadhapalli, V. K. Elumalai, S. Shivram, S. Shah, and D. Mahajan, "Deep reinforcement learning with reward shaping for tracking control and vibration suppression of flexible link manipulator," *Appl. Soft Comput.*, vol. 152, Feb. 2024, Art. no. 110756.
[17] G. Cui, B. Li, W. Tian, W. Liao, and W. Zhao, "Dynamic modeling and vibration prediction of an industrial robot in manufacturing," *Appl. Math. Model.*, vol. 105, pp. 114–136, May 2022.
[18] H. Vieler, A. Karim, and A. Lechler, "Drive based damping for robots with secondary encoders," *Robot. Computer-Integrated Manuf.*, vol. 47, pp. 117–122, Oct. 2017.
[19] D. Feliu-Talegon and V. Feliu-Batlle, "Control of very lightweight 2-DOF single-link flexible robots robust to strain gauge sensor disturbances: A fractional-order approach," *IEEE Trans. Control Syst. Technol.*, vol. 30, no. 1, pp. 14–29, Jan. 2022.
[20] S. Gharab, S. Benftima, and V. F. Batlle, "Fractional control of a lightweight single link flexible robot robust to strain gauge sensor disturbances and payload changes," *Actuators*, vol. 10, no. 12, p. 317, Nov. 2021.
[21] Y. She, Z. Gu, S. Song, H.-J. Su, and J. Wang, "A continuously tunable stiffness arm with cable-driven mechanisms for safe physical human–robot interaction," in *Proc. 44th Mech. Robot. Conf. (MR)*, vol. 83990, Aug. 2020, pp. 1–21.
[22] Y. She, S. Song, H.-J. Su, and J. Wang, "A parametric study of compliant link design for safe physical Human–Robot interaction," *Robotica*, vol. 39, no. 10, pp. 1739–1759, Oct. 2021.
[23] B. Balachandran and E. B. Magrab, *Vibrations*. Cambridge, U.K.: Cambridge Univ. Press, 2018.
[24] D. Singhal and V. Narayanamurthy, "Large and small deflection analysis of a cantilever beam," *J. Inst. Engineers (India): Ser. A*, vol. 100, no. 1, pp. 83–96, Mar. 2019.
[25] J. Malzahn, A. S. Phung, F. Hoffmann, and T. Bertram, "Vibration control of a multi-flexible-link robot arm under gravity," *IEEE Int. Conf. Robot. Biomimetics*, vol. NA, pp. 1249–1254, Dec. 2011.
[26] *KUKA*. Accessed: Mar. 26, 2024. [Online]. Available: https://www.kuka.com/en-de/products/robot-systems/industrial-robots/lbr-iiwa .
[27] C. R. Trends, "Collaborative robots comparison tool," *CobotTrends*, vol. 15, no. 3, pp. 238–253, Sep. 2024. [Online]. Available: https://www.cobottrends.com/cobot-comparison-tool/
[28] O. S. Martin P. Bendsøe, *Topology Optimization; Theory, Methods, and Applications*. Cham, Switzerland: Springer, 2004.
[29] K. Langlois, T. van der Hoeven, D. Rodriguez Cianca, T. Verstraten, T. Bacek, B. Convens, C. Rodriguez-Guerrero, V. Grosu, D. Lefeber, and B. Vanderborght, "EtherCAT tutorial: An introduction for real-time hardware communication on windows [tutorial]," *IEEE Robot. Autom. Mag.*, vol. 25, no. 1, pp. 22–122, Mar. 2018.
[30] S. Derby, "The deflection and compensation of general purpose robot arms," *Mechanism Mach. Theory*, vol. 18, no. 6, pp. 445–450, Jan. 1983. [Online]. Available: https://www.sciencedirect.com/science/article/pii/0094114X83900605
[31] S. S. Rao and F. F. Yap, *Mechanical Vibrations*, vol. 4. Reading, MA, USA: Addison-Wesley, 1995.
[32] Z. Pan and H. Zhang, "Analysis and suppression of chatter in robotic machining process," in *Proc. Int. Conf. Control, Autom. Syst.*, 2007, pp. 595–600.
[33] R. Pintelon and J. Schoukens, *System Identification: A Frequency Domain Approach*. Hoboken, NJ, USA: Wiley, 2012.
[34] *Manipulating Industrial Robots—Performance Criteria and Related Test Methods*, T. B. S. Institution, Toulouse, France, 2016.
[35] M. Iskandar, C. Ott, A. Albu-Schäffer, B. Siciliano, and A. Dietrich, "Hybrid force-impedance control for fast end-effector motions," *IEEE Robot. Autom. Lett.*, vol. 8, no. 7, pp. 3931–3938, Jul. 2023.
[36] O. Felix Offodile and K. Ugwu, "Evaluating the effect of speed and payload on robot repeatability," *Robot. Computer-Integrated Manuf.*, vol. 8, no. 1, pp. 27–33, Jan. 1991. [Online]. Available: https://www.sciencedirect.com/science/article/pii/073658459190004C
[37] *Robots and Robotic Devices-Collaborative Robots*, T. B. S. Institution, Toulouse, France, 2016.
[38] (2021). *Universal Robots E-series User Manual*. [Online]. Available: https://s3-eu-west-1.amazonaws.com/ur-support-site/61707/99473_UR16e_User_Manual_en_Global.pdf
[39] T. R. Kurfess, *Robotics and Automation Handbook Book*, vol. 414. Boca Raton, FL, USA: CRC Press, 2005.

THIERRY HUBERT received the master's degree in industrial engineering from the Vrije Universiteit Brussel, in July 2020, where he is currently pursuing the Ph.D. degree with the Robotics and Multibody Mechanics Research Group. His research focuses on the weight optimization of robotic structures without stiffness constraints and vibration control.

AMIN KHORASANI received the bachelor's degree in mechanical engineering from Babol Noshirvani University of Technology and the master's degree in mechatronics engineering from the K. N. Toosi University of Technology, in 2016. Since 2021, he has been a Ph.D. Researcher with the Robotics and Multibody Mechanics (RMM) Research Group, VUB. His research focuses on designing and developing redundant actuators for cobot applications.

MUHAMMAD USMAN received the B.S. degree in electrical engineering from the National University of Science and Technology, Pakistan, in 2015, and the master's degree in mechanical engineering from Korea University of Technology and Education, South Korea, in 2018. He is currently pursuing the Ph.D. degree with the Robotics and Multibody Mechanics Research Group, Vrije Universiteit Brussel, Belgium. His research interests include compliant actuators, actuator design, and collaborative robots.

HAFSA NOUHI received the joint master's degree in electromechanical engineering from the Vrije Universiteit Brussel and the Université Libre de Bruxelles, in September 2023. She is currently pursuing the Ph.D. degree with the Robotics and Multibody Mechanics Research Group, Vrije Universiteit Brussel. Her research interests include safe human–robot interaction, lightweight robots, and control design.

RAPHAËL FURNÉMONT received the joint degree in mechanical engineering from the Vrije Universiteit Brussel, Belgium, and the Université Libre de Bruxelles, Brussels, Belgium, in 2013, and the Ph.D. degree from the Vrije Universiteit Brussel, in 2019. He is currently a Postdoctoral Researcher at the Robotics and Multibody Mechanics Research Group. His research interests include compliant actuation, energy-efficient actuation, and optimal control.

JOHN LATAIRE (Member, IEEE) was born in Brussels, Belgium, in 1983. He received the Electrical Engineering degree in electronics and information processing and the Ph.D. degree in engineering sciences (Doctor in de Ingenieurswetenschappen) from the Vrije Universiteit Brussel, Brussels, in 2006 and 2011, respectively. From October 2007 to October 2011, he was on a Ph.D. fellowship from the Research Foundation—Flanders (FWO). Since 2022, he has been an Associate Professor at the Department ELEC, VUB. He is the co-author of more than 50 articles in refereed international journals. His main research interests include the frequency domain formulation of the identification of dynamic systems, with a specific focus on the identification of time-varying systems, and the use of kernel-based regression in system identification. He received the 2008 IOP Outstanding Paper Award (Best Paper in Measurement Science & Technology) and the Best Junior Presentation Award 2010 at the 29th Benelux Meeting on Systems and Control and was a co-recipient of the 2014 Andy Chi award (Best Paper in IEEE Transaction on Instrumentation and Measurement). He was a recipient of the 2016 J. Barry Oakes Advancement Award (from the IEEE Instrumentation and Measurement Society).

BRAM VANDERBORGHT received the Ph.D. degree from the Vrije Universiteit Brussel, in 2007. Since 2009, he has been a Professor at VUB. He is affiliated with imec, Belgium, as Scientific Collaborator. He had an ERC starting grant and has coordinated three EU projects on smart and self healing materials for soft robots. He performed research at JRL Laboratory, AIST, Tsukuba, Japan, and did his postdoctoral research at Italian Institute of Technology. His research interests include human–robot collaboration for applications for health and manufacturing, such as exoskeletons, prostheses, social robots, drones, and cobots.

GREET VAN DE PERRE received the degree in mechanical engineering from the Vrije Universiteit Brussel, in June 2011, and the Ph.D. degree in social robotics, in 2018. She is currently a Postdoctoral Researcher and an Associate Professor at the Robotics and Multibody Mechanics Research Group, Vrije Universiteit Brussel. She was granted a scholarship from the Research Foundation-Flanders (FWO). She is working on flexible link manipulators for collaborative robotics funded by an FWO Junior Postdoctoral Fellowship. Her research interests include human–robot interaction, collaborative robotics, and lightweight robotics.

TOM VERSTRATEN (Member, IEEE) received the master's degree in electromechanical engineering and the Ph.D. degree from Vrije Universiteit Brussel (VUB), in 2012 and 2018, respectively. He was a Visiting Researcher at TU Darmstadt, Germany, in 2017, and at the University of Tulsa, USA, from 2018 to 2019. He is currently a Professor at the Robotics and Multibody Mechanics Research Group, VUB. He was awarded fellowships of the Research Foundation-Flanders (FWO) for both his Ph.D. and postdoctoral research. For this research stay, he was awarded a Fulbright Grant for visiting scholars. His research is focused on the study and development of energy-efficient actuators for applications with varying loads and speeds. His research interests include elastic actuators and redundant actuation.